Montmorillonite colloids: II. Colloidal size dependency on radionuclide adsorption

Knapp Karin Norrfors, Remi Marsac, Muriel Bouby, Stephanie Heck, Susanna Wold, Johannes Lützenkirchen, Thorsten Schäfer

Montmorillonite colloids: II. Colloidal Size Dependency on Radionuclide Adsorption

Knapp Karin Norrfors*[1,2], Rémi Marsac[1], Muriel Bouby[1], Stephanie Heck[1], Susanna Wold[2], Johannes Lützenkirchen[1] and Thorsten Schäfer[1]

1: Karlsruhe Institute of Technology (KIT), Institute for Nuclear Waste Disposal (INE), P.O. Box 3640, D-760 21 Karlsruhe, Germany

2: School of Chemical Science and Engineering, Applied Physical Chemistry, KTH Royal Institute of Technology, Teknikringen 30, SE-100 44 Stockholm, Sweden

*Corresponding author. E-mail: norrfors@kth.se (K.K. Norrfors) Tel: +46 8 7909279. Fax: +46 8 7908772.

Keywords

Montmorillonite colloids, particle size effect, adsorption, radionuclides, nuclear waste disposal

Abstract

Bentonite is a strong radionuclide (RN) adsorbent. As a consequence, it is proposed as one of the engineered safety barriers in many concepts of nuclear waste disposal in granite formations. Nevertheless, in contact with groundwater of low ionic strength, montmorillonite colloids may be released from the bentonite buffer and transported towards the biosphere. During the transport of colloids in bedrock fractures, size separation of clay colloids may occur, that may potentially also affect the RN mobility. In this work, the RN adsorption (Th(IV), U(VI), Np(V), Tc(VII) and Pu(IV)) onto size fractionated montmorillonite colloids was studied in a synthetic, carbonated groundwater. We combined batch adsorption experiments and geochemical modelling. U(VI), Np(V) and Tc(VII) did not adsorb to the montmorillonite colloids in the synthetic groundwater. Adsorption of Th(IV) and Pu(IV) was strong but, within experimental uncertainties, not significantly affected by the mean colloidal size. In this case, average K_D values could in principle be used in reactive transport modelling. Montmorillonite clay colloids obtained by fractionation of the raw clay material but in the presence of organic matter during the initial separation step exhibited significantly reduced affinity for Th and Pu.

1 Introduction

The deep geological repository concept for high-level nuclear waste includes several barriers (technical, geotechnical and geological) to isolate or retard the potential transport of radionuclides (RNs) towards the biosphere. Compacted bentonite is planned to be the geotechnical barrier surrounding the metal canisters (SKB, 2010). Bentonite consists mainly of montmorillonite (smectite clay) and is chosen for its favourable swelling capacities, its high cation adsorption capacities and its strong mechanical stability (Karnland et al., 2006). In case of canister failure, this geotechnical barrier will retard the RN transport towards the biosphere. However, in contact with groundwater of low ionic strength, the bentonite barrier may release stable montmorillonite colloids (Geckeis et al., 2004; Missana et al., 2003; Schäfer et al., 2012). The montmorillonite colloids can be transported through the geosphere via advective water flows (Möri et al., 2003). To be able to estimate the colloid facilitated transport of RNs, a large and complex set of parameters has to be considered.

Colloidal transport of montmorillonite through bedrock fractures depends on the ground water flow velocity (Zhang et al., 2012). At high water flow velocity, i.e. in clean bedrock fractures with a low amount of fracture filling material (FFM), a laminar water flow is expected which can separate the colloids according to their mass (for the same specific density), and thus their size. In the opposite, if the fracture contains sufficient amount of FFM, the FFM may be simplified seen as a porous medium, where larger colloids can be transported in the fastest streamlines due to size exclusion effects (Bradford et al., 2002; Sirivithayapakorn and Keller, 2003). Since size separation of montmorillonite colloids may occur in bedrock fractures, their size, morphology, stability and RN adsorption capacities are some of the important parameters for estimating colloid facilitated transport of RNs. These parameters should therefore be included in reactive transport modelling. In a recent study on montmorillonite colloidal stability performed at various ionic strengths (Norrfors et al., 2015), no dependency on the montmorillonite size could be observed. Based on this study, hydrodynamic induced size fractionation and the potential formation of different colloid size fractions will not influence their stability under the same geochemical conditions but some colloids may be able to migrate further due to e.g. steric stabilisation effects by natural occurring dissolved organic matter as fulvic acid (FA).

It is of high importance to examine how the RN adsorption depends on the clay colloid size and thus, the total exposed surface area. Previous studies have demonstrated a size-dependent reactivity of hematite nano-mineral surfaces on Cu^{2+} adsorption (Madden et al., 2006). If the RN adsorption is shown to depend on the montmorillonite colloidal size, owing to their exposed lateral surface area, the amount of RNs transported through the bedrock would be over- or underestimated in the reactive transport models used today (Vahlund and Hermansson, 2006). Alternatively, if the exposed surface area does not have a large impact on the adsorption capacities, averaged adsorption capacities for montmorillonite can be used, as in the case of cation exchange, which is thought to be independent of colloidal size (Stul and Van Leemput, 1982). Tournassat et al. (Tournassat et al., 2003) suggested a model where the amount of edge sites can be calculated from the aspect ratio and the density of the clay particles by assuming a site density of silanol and aluminol edge sites per mass clay. Given the same density of all clay particles, the amount of edge sites are proportional to the aspect ratio. This model was further developed by the authors in a previous work (Norrfors et al., 2015) where montmorillonite colloids were successfully separated into fractions with varying mean colloid sizes. These colloids were used in the adsorption study presented in this work.

Accordingly, this work aims to investigate the influence of the exposed lateral surface area of montmorillonite colloids (which is related to their size) on the adsorption of trace concentrations of RNs in a synthetic groundwater (SGW) representing a glacial meltwater type (Geckeis et al., 2004; Kunze et al., 2008; Möri et al., 2003). In this work, the term clay colloids refer to aggregates, consisting of stacks of several clay mineral layers. Seven montmorillonite dispersions with different mean particle sizes, including one containing fulvic acids (FA), were used for adsorption studies with ^{232}Th(IV), ^{99}Tc(VII), ^{233}U(VI), ^{237}Np(V) and ^{242}Pu(IV) during a long (up to six months) equilibration time. The 2 sites protolysis non-electrostatic surface complexation and cation exchange (2 SPNE SC/CE) model (Bradbury and Baeyens, 2011) was used to predict the uptake of RNs. In addition, we attempted to estimate the influence of expected amounts of edge sites, calculated for each particle size, on the RN adsorption process.

2 Material and Methods

2.1 Montmorillonite colloids and fulvic acids

Various dispersions containing size fractionated montmorillonite colloids originating from raw Wyoming MX80 bentonite (M_w = 372.6 g/mol (Karnland et al., 2006)), American Colloid Co., were used in this study. Preparation and characterization of the montmorillonite dispersions are explained in detail in previous work (Norrfors et al., 2015). A summary of the preparation protocol is presented schematically in Figure 1. Details of centrifugation speeds and times are given in Table 1. In brief, the un-purified MX80 bentonite (10 g/L) was placed into carbonated synthetic groundwater (SGW) and settled during three days. The supernatant was collected and named dispersion S0. The dispersion S0 was further separated into different size fractions by sequential or direct centrifugation. In the sequential (ultra-)centrifugation, S0 was first centrifuged to obtain supernatant S1. Thereafter, S1 was centrifuged to obtain supernatant S2 etc., resulting as well in supernatants S3 and S3.5. For comparison, S0 was also directly ultra-centrifuged (UC) to obtain the dispersion $S3.5^{UC}$. It was found that the dispersions S3.5 and $S3.5^{UC}$ exhibit the same size distribution of colloids despite the different separation protocol. All dispersions have been characterized according their size, chemical composition, mineralogical composition and colloidal concentration in a previous paper, where all details can be found (Norrfors et al., 2015). Suspension concentration was adjusted to 20 mg/L in the RN batch adsorption experiments.

To be able to estimate the exposed lateral surface and thus the amount of adsorption edge sites in each montmorillonite dispersions, the clay particles were assumed to be disc-shaped (Norrfors et al., 2015). Then, their mean disc diameter and height were calculated by equations developed by Jennings and Parslow (Jennings, 1993; Jennings and Parslow, 1988). For this purpose, the mean colloidal sizes of each dispersion measured by different techniques were used in the equations to obtain the mean disc sizes and heights, see Table 1 and (Norrfors et al., 2015). These diameters are mean values for the whole size distribution of colloids in the respective dispersions. S0 includes both larger and smaller sized colloids, whereas S3.5 and $S3.5^{UC}$ only include smaller colloids and were therefore less polydisperse.

The amount of adsorption edge sites was calculated according to the work of White and Zelazny (White and Zelazny, 1988) and Tournassat et al. (Tournassat et al., 2003), assuming a clay density of 2.7 g/cm³. The calculated mean clay particle disc diameters were used to determine their lateral area from which the amount of sites in the clay dispersions could be estimated (in mmol/kg). The estimated amounts of sites are presented in Table 1.

Complementary, one clay suspension was prepared in presence of FA, representing natural organic matter. The fulvic acid (FA-573) has been extracted from a natural groundwater (Gohy573) of the Gorleben site, Germany (Wolf et al., 2004). A small amount of FA was weighed, dissolved in NaOH and diluted in a separate clay dispersion (10 g raw MX80 bentonite in 1 L SGW). Thereafter, this FA-clay dispersion was ultra-centrifuged during the same time and at the same speed as the dispersion $S3.5^{UC}$, and denoted $S3.5^{UC,FA}$. The final concentration of FA in the batch adsorption experiment was approximately 1.9 mg/L after dilution of the dispersion $S3.5^{UC,FA}$ to a concentration of 20 mg/L montmorillonite colloids.

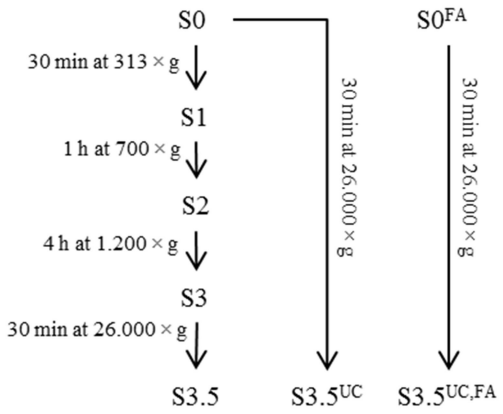

Figure 1: Schematic diagram of bentonite fractionation into various aggregate size fractions by sequential and direct (ultra-)centrifugation.

Table 1: Dispersions used in the batch adsorption experiments, separation protocol performed, mean diameter of the clay discs and amounts of adsorption sites determined (Norrfors et al., 2015).

Colloidal dispersion	Conditions of separation (C: centrifugation; UC: ultracentrifugation)	Mean diameter of clay discs (nm)	Amount of adsorption sites (mmol/kg)
S0	3 days sedimentation	1496	11.2
S1	C: 30 min (S0) at 313 × g	940	17.8
S2	C: 1 h (S1) at 700 × g	500	33.5

S3	C: 4 h (S2) at 1.200 × g	250	67.0
S3.5	UC: 30 min (S3) at 26.000 × g	258	64.7
S3.5^{UC}	UC: 30 min (S0) at 26.000 × g[a]	246	67.9
S3.5^{UC,FA}	UC: 30 min (S0) at 26.000 × g[a]	187	89.5*

[a]: one step ultra-centrifugation from colloidal dispersion S0 obtained after stirring and sedimentation of a MX80 dispersion at 10 g/L in presence or absence of 11.8 mg/L FA . *: Amount of sites estimated from the mean colloidal size, i.e. neglecting potential site occupancy by FA.

2.2 Synthetic Groundwater (SGW)

Synthetic, carbonated groundwater (SGW) is used as background electrolyte to simulate a glacial meltwater of low ionic strength, similar to the granitic groundwater present at the Grimsel Test Site (Geckeis et al., 2004; Kunze et al., 2008; Möri et al., 2003). The SGW is prepared by mixing different salts (NaCl, $CaCl_2$, $MgCl_2$, NaF, Na_2SO_4 and $NaHCO_3$), yielding the composition presented in Table 2. The total ionic strength is 1.6 mM and the pH is 8.4 ± 0.1 prior to contact with montmorillonite colloids and radionuclide cocktail.

Table 2: The chemical composition of the synthetic groundwater (SGW) used as background electrolyte in all samples (Norrfors et al., 2015).

Element	**Concentration (mM)**
Na^+	1.2
Ca^{2+}	0.05
F^-	0.1
Cl^-	0.074
SO_4^{2-}	0.04
HCO_3^-	1.0
pH	8.4 ± 0.1

$Eh_{(SHE)}$	+0.35 ± 0.05 V

2.3 Radionuclide cocktail

A radionuclide cocktail containing the elements: ^{232}Th, ^{99}Tc, ^{233}U, ^{237}Np and ^{242}Pu was prepared in a glove box under Ar atmosphere in 0.1 M HCl. The cocktail was used to spike the seven clay dispersions, diluted to 20 mg colloids/L in the SGW. The initial (total) RN concentrations in all adsorption samples was checked by analysing the top 0.5 mL out of a total sample volume of 50 mL by ICP-MS. This yielded [$^{232}Th(IV)$] = 10^{-8} M, [$^{99}Tc(VII)$] = $5 \cdot 10^{-9}$ M, [$^{233}U(VI)$] = 10^{-8} M, [$^{237}Np(V)$] = 10^{-8} M and [$^{242}Pu(IV)$] = $2 \cdot 10^{-9}$ M. ^{242}Pu was added as $^{242}Pu(III)$ to the radionuclide cocktail, but based on thermodynamic considerations, Pu(III) was expected to oxidize to Pu(IV) due to pH adjustments under the SGW experimental conditions utilized, as will be further discussed in section 3.1.6. All RNs concentrations (expect for Pu) were below the relative solubility limits in the carbonated SGW, according to literature (Np(V) (Guillaumont and Mompean, 2003; Neck et al., 1992; Runde et al., 2002), Tc(VII) (Alliot et al., 2009), U(VI) and Pu(IV) (Huber et al., 2011), Th(IV) (Östhols et al., 1994)).

2.4 Experimental conditions and procedure

All experiments were performed at room temperature in a glove box under Ar atmosphere (<1 ppm O_2). pH was measured with a semi micro Ross electrode (81-03, Orion Co.) in combination with a digital pH-meter (720A, Orion Co.). This set-up was calibrated using four commercial buffer solutions (Merck). The redox potentials in the clay dispersions were measured using an Orion 525A (Eh meter) and a Pt electrode combined with Ag/AgCl reference system (Metrohm). Raw data were converted into Eh vs. standard hydrogen electrode (SHE) by correcting for the potential of the reference electrode. A commercial redox-buffer (+220 mV, Schott instruments) was used for calibration. An equilibration time of 30 min was applied for all Eh measurements. Uncertainties in Eh measurements were ± 50 mV (Altmaier et al., 2010; Kirsch et al., 2011).

Each batch adsorption sample was prepared in duplicate and contained 20 mg/L montmorillonite in a total volume of 50 mL. For monitoring radionuclide adsorption, aliquots

of the samples were taken after 72 h (~3 days), 260 h (~2 weeks), 580 h (~1 month) and 3800 h (~6 months). Initially, the top 0.5 mL of the sample was analysed by ICP-MS to obtain the amount of stable montmorillonite colloids in the dispersion. Thereafter, approximately 4 mL of each sample was transferred into ultra-centrifugation vials, sealed by welding inside the glove box and afterwards ultra-centrifuged (Beckman XL-90, rotor type 90Ti) for 1h at 90.000 rpm (centrifugal force of approximately $7 \cdot 10^5 \times g$). Subsequently, a volume of 0.5 mL of the ultra-centrifuged supernatants was sampled and analysed by ICP-MS. This ultra-centrifugation procedure has been proven to effectively remove montmorillonite colloids and thereby the RNs associated to colloids (Altmaier et al., 2004). When the experiment ended (i.e. after 6 months), all samples were characterised by pH = 8.9 ± 0.3 and $Eh_{(SHE)}$ = +230 ± 50 mV.

From the ICP-MS data, the distribution of RNs was calculated and defined as (i) the amount of soluble species RNs in dispersion (%Free), (ii) RNs associated to montmorillonite colloids (%Colloid) and (iii) the amount of RNs associated to particulates (i.e. settled particles, %Part). This is illustrated in Figure 2. When present initially, 70% of the FA was found free in the dispersion after fractionation. No distinction between soluble RNs species and dissolved FA-RN complexes could be made with this method. The concentration of RNs as soluble species was measured in the supernatant after ultra-centrifugation. Colloidal RN concentration was determined from the difference in concentration before and after ultra-centrifugation. Particulate RNs was the remaining RN concentration based on the initial concentration. All results presented are mean values of duplicate samples with its standard deviation. The dispersion S3.5 was proved to have the same size distribution as $S3.5^{UC}$. Identical adsorption results were obtained for these two dispersions, indicating a good reproducibility of the fractionation procedure developed (Norrfors et al., 2015).

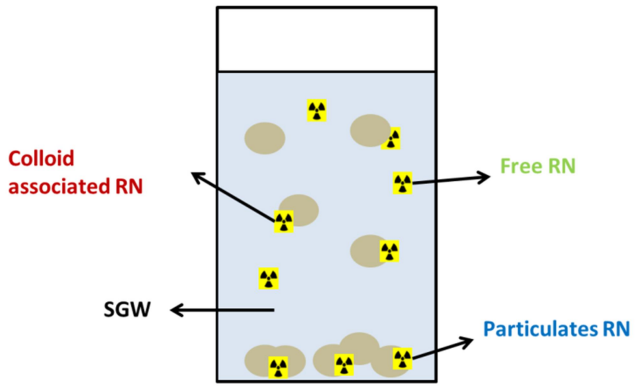

Figure 2: Schematic diagram of the radionuclide (RN) distribution in the batch adsorption samples, as determined from ICP-MS measurements.

K_D values for each RN were calculated for the overall RN adsorption as "average K_D values", which does not distinguish between suspended (%Colloids) and particulate (settled particles, %Part) clay. The expression for K_D is given in equation 1:

$$K_D = \frac{[RN]_{Tot} - [RN]_{free}}{[RN]_{free}} \cdot \frac{1}{m_{Clay}} \; (dm^3/kg) \quad (1)$$

where $[RN]_{Tot}$ and m_{Clay} are the total, initial concentrations of RNs and montmorillonite, respectively. $[RN]_{free}$ is the concentration of soluble species of RNs in solution after a given equilibration time. A standard deviation of log (K_D (dm^3/kg)) = 0.5 was applied to all K_D values, as suggested by Bradbury and Baeyens (Bradbury and Baeyens, 2011), due to experimental uncertainties for strongly adsorbing elements.

Additionally, with the mean amount of adsorption sites estimated for each clay dispersion, a K_D value normalized to the amount of sites ($K_{D,sites}$) was calculated. The relationship between the mass-normalized (K_D), the sites-normalized values ($K_{D,sites}$) and the amount of sites in one clay dispersion ([Sites]) is given by equation 2:

$$\log K_{D,sites} \; (dm^3/mol\; of sorption\; sites) = \log K_D \; (dm^3/kg) - \log[Sites] \; (mol/kg) \quad (2)$$

As mentioned above, the montmorillonite dispersions (S0 and S1) containing the largest sized clay particles contain a mixture of colloidal sizes. In these dispersions, the larger clay particles sediment with time, whereas the smaller clay colloids will remain suspended. Therefore, a better evaluation of RN adsorption onto different colloid sizes could be made in these dispersions if the average K_D value was compared to the K_D value for the particulates (settled, large particles) in the clay dispersion, i.e. $K_{D,part}$, defined as:

$$K_{D,part} = \frac{[RN]_{Tot} - [RN]_{free} - [RN]_{colloid}}{[RN]_{free}} \cdot \frac{1}{m_{part}} \; (dm^3/kg) \quad (3)$$

where $[RN]_{colloid}$ is the amount of RNs associated to stable, suspended clay colloids and m_{part} the amount of clay particulates.

2.5 Geochemical speciation modelling

Predominance diagrams were plotted with PhreePlot (Kinniburgh and Cooper, 2009), which contains an embedded version of the geochemical speciation program PHREEQC (Parkhurst and Appelo, 1999). Stability constants for dissolved species and solubility calculations were included in the NEA database (U/Np/Pu: (Guillaumont and Mompean, 2003), Tc: (Rard, 1999), Th: (Rand et al., 2009)). Fluoride and carbonate complexes for all RNs were considered in the calculations. However, at the present chemical conditions, the fluoride complexes did not play a significant role for the speciation. The formation constants of $Pu(OH)_2(CO_3)_2^{2-}$ and $Np(OH)_2(CO_3)_2^{2-}$ selected by THEREDA (Release 2013-08-02) were used in all calculations. The selected constants (in the NEA and THEREDA databases) were consistent with each other. The Davies equation was used for activity coefficient calculations. Reduction of sulfate and CO_2 was not considered in the calculations.

The cation exchange capacity (CEC) was estimated to 0.87 eq/kg by Marques Fernandes et al. (Marques Fernandes et al., 2012). With the available adsorption constants, preliminary tests with all RNs showed that cation exchange reactions had no significant influence at pH 8.9. Consequently, cation exchange reactions were neglected in the present study.

To predict adsorption on natural clay rocks, Bradbury and Baeyens (Bradbury and Baeyens, 2011) applied a linear additive model (LAM). Their "bottom-up" approach describes the overall adsorption of an element to a complex mineral mixture as the sum of the amount adsorbed to each single type of mineral. For bentonite, they considered montmorillonite as the only adsorbent for radionuclides. In the present case, montmorillonite represents 75 wt.% of MX80 bentonite. Bradbury and Baeyens developed the 2 Site Protolysis Non Electrostatic Surface Complexation and Cation Exchange (2SPNE SC/CE) model for surface complexation and cation exchange reactions at montmorillonite surfaces (Bradbury and Baeyens, 2005; Bradbury and Baeyens, 2006). Two types of proton active sites were necessary to describe the titration data, but only one type was assumed to bind cations by the model approach. The cation binding sites consist of weak sites ($[\equiv WOH] = 4 \cdot 10^{-2}$ mol/kg) as well as less abundant strong sites ($[\equiv SOH] = 2 \cdot 10^{-3}$ mol/kg) with identical acid-base properties. Bradbury and Baeyens (Bradbury and Baeyens, 2005; Bradbury and Baeyens, 2006) determined surface complexation constants for Np(V), U(VI) and Th(IV) to strong sites of montmorillonite. Due to the low RN concentrations investigated in this study and the lack of RN surface complexation constants for the weak sites, only the strong sites were considered as adsorption

sites. In solution, all RNs were predominately present as neutral or negative species due to complexation with OH^-/CO_3^{2-}. Marques-Fernandez et al. (Marques Fernandes et al., 2012) determined thermodynamic constants for the formation of ternary montmorillonite-U(VI)-carbonate surface complexes. Ternary montmorillonite-Np(V)-carbonate surface complexes were not observed (Turner et al., 1998). Adsorption of TcO_4^- to clays can be neglected (Guillaumont and Mompean, 2003; Ticknor et al., 1996).

Though added in oxidized form, Np(V) might be reduced to Np(IV) at the clay surface in line with work by Marsac et al. (Marsac et al., 2015) in the Np-illite system. Np(IV) adsorbs more strongly to minerals than the oxidized form. Surface complexation constants for Np(IV) are unknown for montmorillonite, but Bradbury and Baeyens (Bradbury and Baeyens, 2005; Bradbury and Baeyens, 2009) proposed linear free energy relationships (LFER) between cation hydrolysis constants (equation 4) and surface complexation constants (equation 5) for illite and montmorillonite within the 2SPNE SC/CE model.

$$M^{n+} + xH_2O \rightleftharpoons M(OH)_x^{(n-x)} + H^+, \text{ giving } {}^{OH}K_x \quad (4)$$

$$\equiv \mathrm{SOH} + M^{n+} + (x-1)H_2O \rightleftharpoons \equiv \mathrm{SOM(OH)}_{(x-1)}^{(n-x)} + xH^+, \text{ giving } {}^{S}K_{(x-1)} \quad (5)$$

The LFERs for montmorillonite (equation 6) and illite (equation 7) are:

$$\log {}^{S}K_{(x-1),mont} = 8.1 + 0.90 \times \log {}^{OH}K_x \quad (6)$$

$$\log {}^{S}K_{(x-1),ill} = 7.9 + 0.83 \times \log {}^{OH}K_x \quad (7)$$

Uncertainties associated to the parameters of the LFERs were omitted for simplicity. According to Marsac et al. (Marsac et al., 2015) the formation of $\equiv SONp(OH)_4^-$ was required to describe Np(IV) adsorption to illite. The same might be true for montmorillonite, as in the Th(IV) case (Bradbury and Baeyens, 2005). Unfortunately, the formation constant of $\equiv SOAn(OH)_4^-$ cannot be estimated by a LFER since the formation constant for the corresponding aqueous species ($An(OH)_5^-{}_{(aq)}$) was not available. Instead, the combination of equations 6 and 7 yielded an illite-montmorillonite LFER, which can be applied to Np(IV), using surface complexation constants determined by Marsac et al. (Marsac et al., 2015):

$$\log {}^{S}K_{(x-1),mont} = 1.08 \times \log {}^{S}K_{(x-1),ill} - 0.46 \quad (8)$$

The Np(IV) constants were used for Pu(IV) because of their similar hydrolysis constants. By analogy with Np(IV), U(IV) and Tc(IV) surface complexes might form at the montmorillonite surface. However, given the lower redox potentials of the U(VI)/U(IV) and Tc(VII)/Tc(IV) couples compared to Np(V)/Np(IV), reduction of U(VI) or Tc(VII) was not expected at the relatively high Eh of our experiments. Thus, U(IV) and Tc(IV) adsorption to montmorillonite was not further considered.

Bradbury and Baeyens (Bradbury and Baeyens, 2005) showed that cations with different chemical behavior (related to their oxidation state) do not compete for the same adsorption sites, and have to be modelled by considering several types of binding sites for the different RNs. The different sites were given the same surface site density. The tetravalent RNs Th(IV), Np(IV) and Pu(IV) were expected to compete for the same strong sites. Applying the concept further, Np(V) and U(VI) have no competitor for their respective sites in our study. The natural occurrence of ^{238}U, was not taken into account in the calculations, which apply only to the ^{233}U added to the clay dispersions. The surface complexation reactions and constants used in the modeling is presented in the Supporting Information (SIF -1), Table S1.

Our simulations were based on the estimations and assumptions discussed above. In addition, the impact of carbonates on the adsorption of most RNs onto clays has not been investigated. For instance, the potential formation of ternary carbonate-RN-surface complexes, as observed for U(IV) (Marques Fernandes et al., 2012) cannot be generally taken into account.

3 Results and Discussion

3.1 Batch adsorption results

3.1.1 Stability of montmorillonite colloids

The montmorillonite colloidal stability was followed via the evolution of the suspended Al-concentration at a given time, relative to the initial Al-concentration. The percentage of stable colloids for the different dispersions after 3 days, 2 weeks, 1 month and 6 months is shown in Figure 3. No significant sedimentation was observed after 3 days in any dispersion except in those containing larger montmorillonite colloids, i.e. S0 and S1. Here, a clear sedimentation was observed at longer times (e.g. only 55% and 82% remain suspended after 6 months for the dispersions S0 and S1, respectively). In previous work (Norrfors et al., 2015), the long

term stability of the undiluted clay dispersions were studied. In that study, 43% and 70% of the colloids remained stable in dispersions S0 and S1 after 2 months without shaking (Norrfors et al., 2015). Similar trends were found here even though the dispersions were diluted to 20 mg/L. Interestingly, the colloidal dispersion obtained after sequential (ultra-) centrifugation (S3.5) and the dispersion obtained from one direct ultra-centrifugation step ($S3.5^{UC}$), have a similar size distribution (Norrfors et al., 2015), showing the same high colloidal stability (Figure 3).

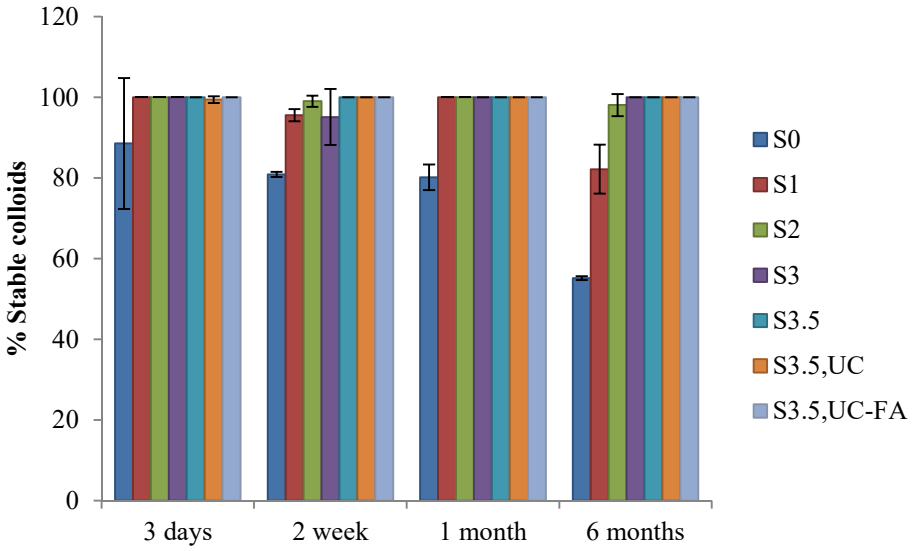

Figure 3: The amount of stable montmorillonite colloids in the seven clay dispersions (Table 1) as a function of time.

3.1.2 Technetium adsorption

Figure 4a shows the predominance pH-Eh diagram for Tc in solution, calculated using Phreeplot. The pH-Eh conditions measured at the end of the experiment (after 6 months, pH = 8.9 ± 0.3 and Eh = 230 ± 50 mV) are shown as a black square and were clearly in the stability field of Tc(VII) (i.e. $TcO_4^-{}_{(aq)}$). Based on this, no reduction of Tc(VII) to Tc(IV) was expected. In addition, no adsorption of Tc was expected due to the low solid to liquid ratio investigated and because of weak adsorption of $TcO_4^-{}_{(aq)}$ onto mineral surfaces (Guillaumont and Mompean, 2003; Huber et al., 2011; Ticknor et al., 1996). Figure 4b presents the distribution of Tc between particulates, suspended colloids and soluble species for the S0 dispersion as a function of equilibration time. Similar results were obtained for all dispersions containing various clay size fractions, as presented in the Supporting Information (SIF -2,

Figure S1). The concentration of Tc(VII) remains constant in solution up to 6 months for all dispersions (Figure 4b and SIF -2, Figure S1). This supports the above statements that no reduction of technetium or adsorption onto clay colloids occurs within the analytical uncertainties, as expected from the speciation calculations. Slow reduction of Tc(VII) to Tc(IV) in presence of synthetic or Febex montmorillonite colloids has previously been noted in natural groundwater of similar low ionic strength (~1 mM) and pH = 9 after 1 month (Huber et al., 2015), which was related to the observed decrease in Eh to approximately -200 mV after 1 month.

Since most FA remains free in dispersion (section 2.4), no distinction between Tc-FA complexes and soluble species of Tc could be done and the Tc distribution in S3.5, S3.5^{UC,FA} and S3.5^{UC} was identical, as expected (SIF -2, Figure S1).

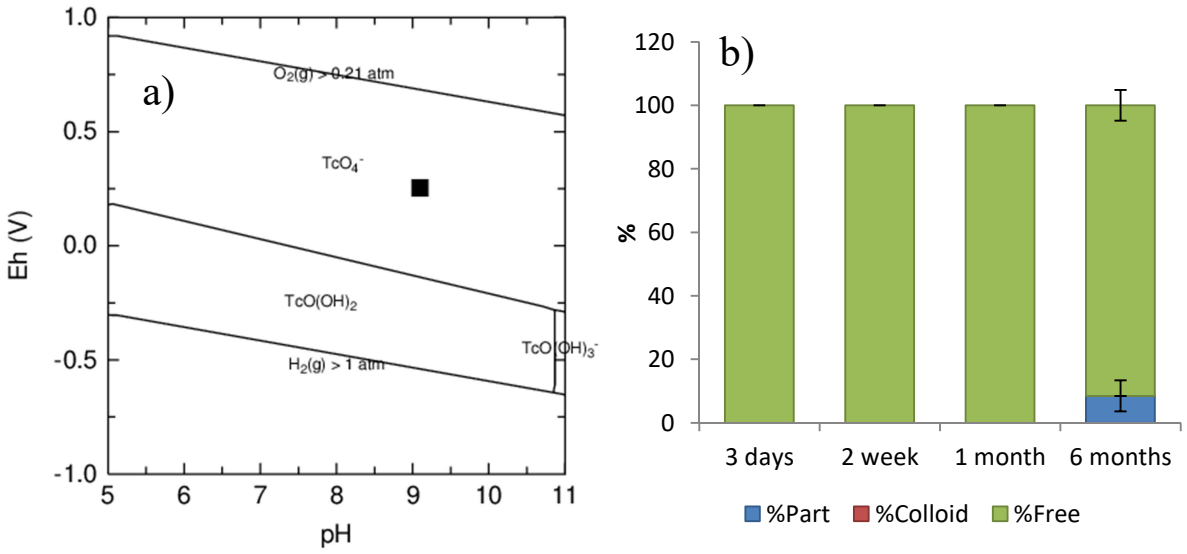

Figure 4: a) Predominance pH-Eh diagram for technetium where the chemical conditions in our study (pH = 8.9 and Eh = 230 mV) are indicated by a black square. b) The distribution of Tc, in percentage, between particulates (%Part, blue), stable clay colloids (%Colloid, red) or soluble species (%Free, green) in the S0 dispersion is shown for different equilibration times. Histograms with the Tc distribution for the other clay dispersions are presented in the Supporting Information (SIF-2, Figure S1).

3.1.3 Uranium adsorption

In the pH-Eh predominance diagram for uranium (Figure 5a) the present experimental conditions (pH = 8.9 ± 0.3 and Eh = 230 ± 50 mV) are indicated by a black square. Due to the presence of carbonate in the SGW, uranium should be mainly present as $UO_2(CO_3)_3^{4-}{}_{(aq)}$.

U(VI) is known to form highly soluble complexes with carbonate at pH 9 (Bernhard et al., 2001; Bradbury and Baeyens, 2011; Hartmann et al., 2008; Marques Fernandes et al., 2012; Regenspurg et al., 2009). In previous studies (Marques Fernandes et al., 2012), a log (K_D (dm^3/kg)) value of 2.7 was presented for U(VI) adsorption onto montmorillonite in 1 mM HCO_3^- and 0.1 M $NaClO_4$ at pH 9. This corresponds to an uptake of 1% uranium with our low clay concentration (20 mg/L). Our simulation for the SGW also predicts ~1% uptake. In Figure 5b, the experimental uranium adsorption for dispersion S0 is presented as the distribution of U between particulates, suspended colloids and soluble species as a function of equilibration time. The results for the other clay dispersions are presented in the Supporting Information (SIF -3, Figure S2). No uranium (^{233}U) adsorption onto montmorillonite was detected, within the experimental uncertainties, in any clay dispersions at any equilibration time. Instead, in line with published studies (Marques Fernandes et al., 2012) and model predictions, uranium remains as soluble carbonate complexes in all clay dispersions. Since FA does not strongly adsorb onto montmorillonite at pH 8.9, the results for dispersion $S3.5^{UC,FA}$ were not expected to differ from those for dispersions in absence of FA, which agrees with the distribution presented (SIF -3, Figure S2).

Interestingly, a significant release of naturally occurring ^{238}U in the raw MX80 clay was observed in all dispersions (SIF-4, Figure S3). This was a consequence of the presence of carbonates in the SGW. This observation further strengthens the assumption that soluble U-carbonate complexes were the favoured species under the present chemical conditions.

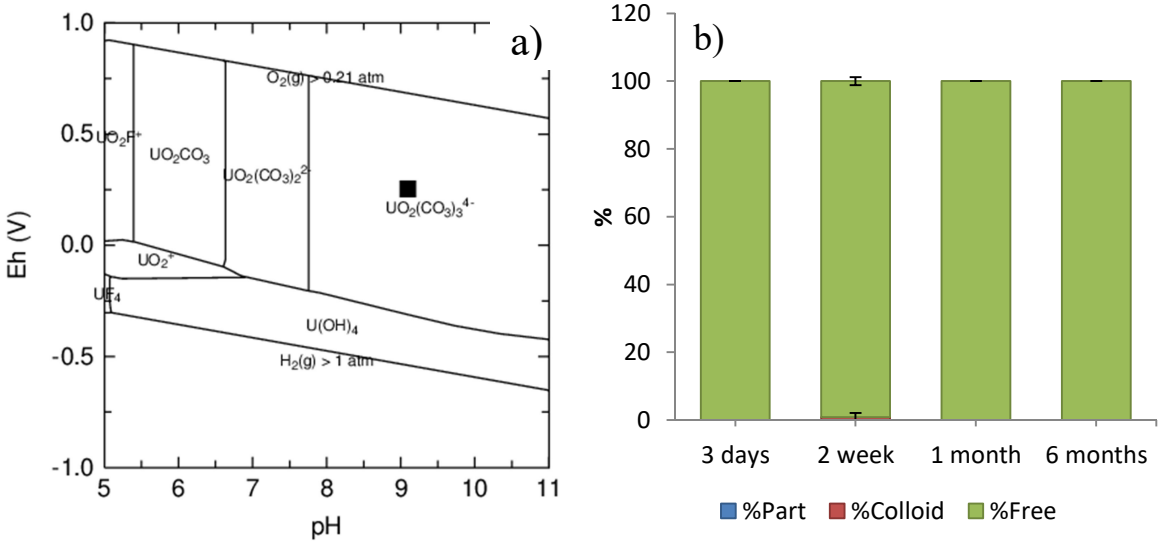

Figure 5: a) Predominance pH-Eh diagram for uranium in the SGW, where the chemical conditions are indicated by a black square (pH = 8.9 and Eh = 230 mV). b) The distribution of U, in percentage, between particulates (%Part, blue), stable clay colloids (%Colloid, red) or soluble species (%Free, green) in the S0 dispersion, shown for different equilibration times. The results obtained for the other clay dispersions are presented in the Supporting Information (SIF -3, Figure S2).

3.1.4 Neptunium adsorption

According to the pH-Eh predominance diagram (Figure 6a), Np should prevail as Np(V) as $NpO_2CO_3^-$ in the SGW (pH = 8.9 and Eh = 230 mV) and remain in solution due to weak Np(V) uptake onto montmorillonite (Missana and Geckeis, 2006; Turner et al., 1998; Wu et al., 2009). The Np distribution in the S0 dispersion is presented in Figure 6b for different equilibration times. The results for the other clay dispersions can be found in the Supporting Information (SIF -5, Figure S4). Overall, as expected, no Np uptake on montmorillonite was detected for any clay dispersion and equilibration time.

Recently, surface induced reduction of Np(V) to Np(IV) in the presence of illite has been evidenced (Marsac et al., 2015). Although Np(V) prevailed in solution, its reduction to Np(IV) was shown to be thermodynamically favoured at the illite surface due to strong Np(IV) adsorption. Structural Fe(II) in illite was suspected to be the redox partner, and Fe(II) is also present in our montmorillonite (Holmboe et al., 2012). Therefore, surface induced reduction of Np(V) to Np(IV) might also be relevant in the case of montmorillonite. Figure 6c shows the predicted percentage of Np uptake by montmorillonite as a function of Eh in the SGW at pH 8.9. For Eh < 50 mV, Np(IV) prevails both at the surface and in solution, leading to nearly complete Np uptake by montmorillonite. For Eh > 300 mV, Np(V) prevails both at the surface and in solution and no uptake was predicted. For 50 < Eh < 300 mV, Np(V) prevails in solution whereas Np(IV) prevails at the surface, leading to an intermediate behaviour, which is highly sensitive to changes in Eh. The measured Eh (+230 mV) is shown as a dashed line, with the experimental uncertainty (± 50 mV), as dotted lines in Figure 6c. The model predicts an uptake of approximately 10% Np at pH 8.9 and $Eh_{(SHE)}$ = +230 mV. However, given the uncertainties in (i) the experimental Eh value and (ii) Np(IV) surface complexation constants reported in the 2 SPNE SC/CE model (Marsac et al., 2015), the experimental Np uptake was qualitatively consistent with the predictions.

As for U and Tc, the presence of FA in S3.5^{UC,FA} did not change the Np uptake as expected, since FA remains predominantly in solution (SIF -5, Figure S4).

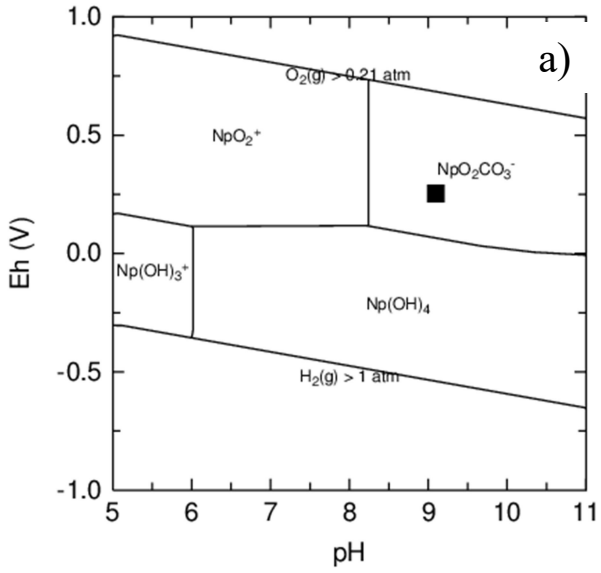

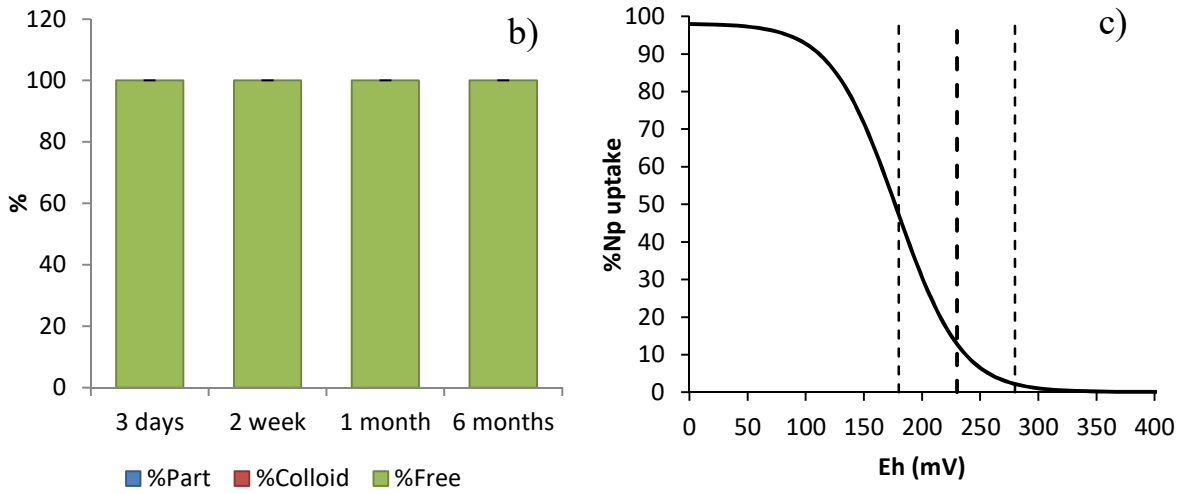

Figure 6: a) Predominance pH-Eh diagram for Np in the SGW. The black square corresponds to the present experimental conditions (pH = 8.9 and Eh = 230 mV). b) Histograms presenting the distribution of neptunium, in percentage, between particulates (%Part, blue), stable colloids (%Colloid, red) or soluble species (%Free, green) in the S0 dispersion shown for different equilibration times. Histograms with the Np distribution for the other clay dispersions are presented in the Supporting Information (SIF -5, Figure S4). c) Predicted percentage uptake of Np by bentonite in the SGW as a function of Eh at pH 8.9. The experimental Eh (230 ± 50 mV) is shown as dashed lines.

3.1.5 Thorium adsorption

The Th speciation in the SGW is shown as a function of pH in Figure 7a. Th was predicted to be present as $Th(OH)_{4(aq)}$ (60%) and $Th(OH)_2(CO_3)_2^{2-}$ (40%) at pH 8.9, marked as a vertical line in Figure 7a. Accordingly, the model predicts 83% of Th(IV) uptake onto montmorillonite, corresponding to log (K_D (dm^3/kg)) = 5.4. The distribution of Th in the S0 dispersion between particulates, suspended colloids or soluble species as a function of equilibration time is presented in Figure 7b. The results for the other clay dispersions are presented in the Supporting Information (SIF -6, Figure S5). Thorium was strongly adsorbed in all clay dispersions. The amount of settled Th increases with time in S0 (Figure 7b). This follows the increase in the amount of depositing clay particles, as already mentioned (Figure 3), pointing to the association of a fraction of Th with those unstable, large montmorillonite particulates. For the clay dispersions containing smaller sized colloids (S2→S3.5^{UC}), no sedimentation was expected which was in line with the experimental results, especially as small amounts of particulates found in all dispersions could rise from artefacts (e.g. adsorption to walls), as this fraction was not measured directly (but calculated from the total amount Th subtracting the measured amounts of Th in colloidal and aqueous phases).

The K_D values calculated for Th in the different clay dispersions are presented as a function of equilibration time in Figure 7c. Data points for samples where the concentration of Th as soluble species were below the detection limit are not shown. Nevertheless, no significant variations in Th uptake was found. Overall, no kinetic effects were observed. Our log (K_D (dm^3/kg)) = 6.4 ± 0.5 were similar to those previously observed. Log (K_D (dm^3/kg)) = 6.4 ± 0.5 and log (K_D (dm^3/kg)) = 5.3 ± 0.5 for batch adsorption experiments were reported by Huber et al. (Huber et al., 2011; Huber et al., 2015) and Bouby et al. (Bouby et al., 2011), respectively, in a low ionic strength (~1 mM) groundwater at pH = 8.3 - 9.5 at carbonate concentrations of ~0.05 mM, comparable to the SGW used in our study. The experimental K_D value was slightly higher than expected from modelling (dashed line in Figure 7c). Nevertheless, the model for Th(IV) uptake was calibrated with the experimental results of Bradbury and Baeyens (Bradbury and Baeyens, 2005), involving a measured log (K_D (dm^3/kg)) ≈ 5.5 for Th at pH = 9 in 0.1 M $NaClO_4$, i.e. in higher ionic strength and in absence of carbonate.

In the montmorillonite dispersion obtained in presence of FA (S3.5^{UC,FA}), the Th uptake onto clay colloids was significantly lower compared to the dispersions in absence of organic matter

(S3.5^{UC}, Figure 7c and SIF -6, Figure S5). Log (K_D (dm^3/kg)) was reduced to 5.3 ± 0.5 and remains constant over time (Figure 7c). FA form complexes with Th(IV) which compete with Th-montmorillonite surface complexes. This K_D value corresponded to a decrease in the amount of adsorbed Th by approximately 15% (see histograms in the Supporting Information, SIF -6, Figure S5). Pan et al. (Pan et al., 2011) reported a decrease in log (K_D (dm^3/kg)) from ~6.0 to ~5.4 after addition of FA in absence of carbonate, at pH = 9 and in 50 mM NaCl, with a FA to Na-bentonite ratio of 1:5 compared to 1:10 in our study. Yu et al. (Yu et al., 2008) reported an even larger decrease in log (K_D (dm^3/kg)) value in presence of FA (from ~5.2 to ~3.9) with a FA to bentonite ratio of 1:30 at pH = 9, at slightly higher ionic strength (0.1 M $NaNO_3$). Therefore, the present results were in line with literature data.

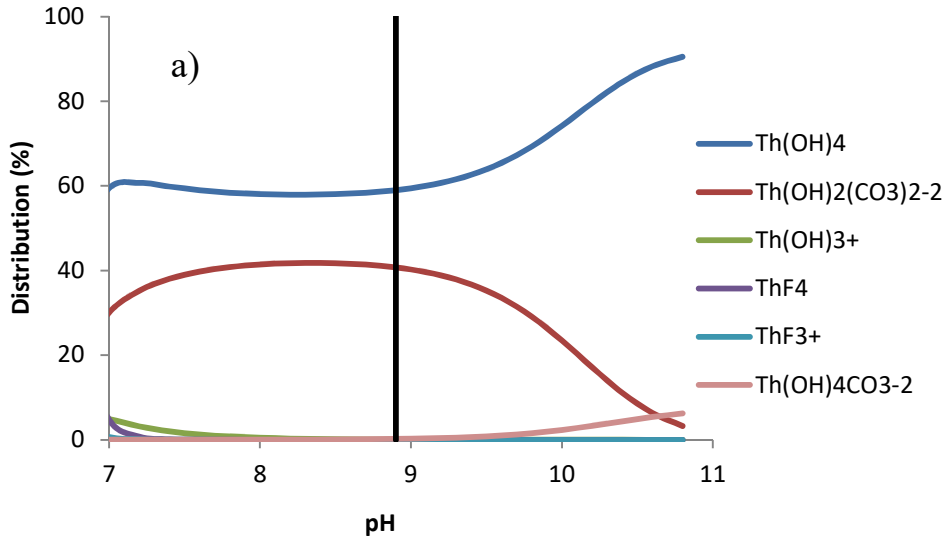

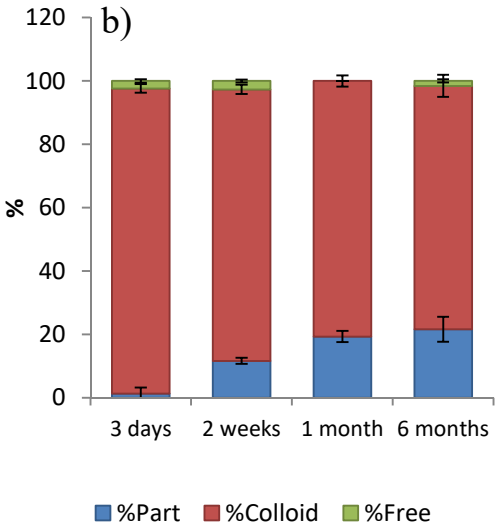

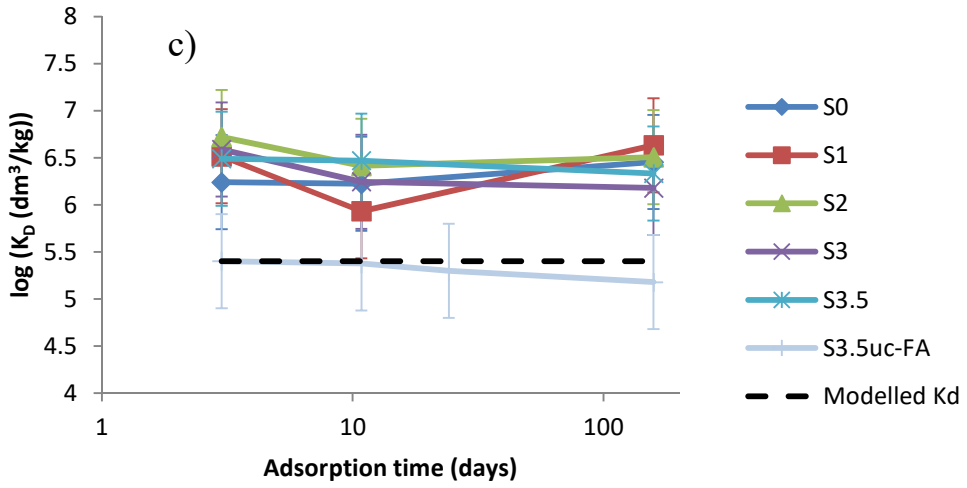

478

479 **Figure 7: a) Species distribution diagram for thorium as a function of pH in the SGW. The experimental**
480 **pH = 8.9 is marked as a vertical line. b) Histograms presenting the distribution of Th, in percentage,**
481 **between particulates (%Part, blue), stable clay colloids (%Colloid, red) or soluble species (%Free, green)**
482 **in the S0 dispersion, shown for different equilibration times. The results obtained for the other clay**
483 **dispersion are presented in the Supporting Information (SIF -6, Figure S5). c) Adsorption of Th for all**
484 **different sized montmorillonite dispersions, expressed as log (K_D (dm^3/kg)) values as a function of**
485 **equilibration time. The dashed line corresponds to the predicted Th adsorption from modelling.**

486

487 ### 3.1.6 Plutonium adsorption

488 In the predominance pH-Eh diagram for Pu (Figure 8a), the experimental conditions are
489 marked by a black square (pH = 8.9 and Eh = 230 mV). In the SGW, Pu was expected to
490 prevail as Pu(IV) mainly as $Pu(OH)_2(CO_3)_2^{2-}{}_{(aq)}$. Pu(IV) is known to adsorb strongly onto
491 montmorillonite (Geckeis et al., 2004; Latrille et al., 2006; Lujanienė et al., 2007). Even
492 though the total amount of Pu would exceed the solubility limit of Pu(IV) (Huber et al., 2011),
493 the final aqueous Pu concentration was below the saturation with respect to $PuO_{2(am,hydr)}$
494 because of the strong adsorption of Pu onto montmorillonite. Furthermore, since adsorption is
495 usually a faster process than nucleation and precipitation, precipitation of Pu was not expected
496 (Zhao et al., 2011). An uptake of 97% Pu(IV) was predicted by the model. This was
497 consistent with the simulated Np uptake at Eh < 50 mV (see Figure 6c), where Np(IV) would
498 prevail both at the surface and in solution. A Pu uptake of 97% corresponds to log (K_D
499 (dm^3/kg)) = 6.3 in our experimental conditions.

500 The distribution of Pu as a function of equilibration time is presented for the clay dispersion
501 S0 in Figure 8b. Pu was largely associated to montmorillonite. The distribution of Pu in the

other clay dispersions is presented in the Supporting Information and was comparable to the results found for S0 (SIF -7, Figure S6 and Figure 8b). As for Th, some Pu is associated to particulates present in the clay dispersions with the largest colloids (i.e. S0 and S1) which is seen over time). This was explained by sedimentation of larger montmorillonite particles (see Figure 3). In the dispersion with smaller colloids, no Pu particulates were found (SIF -7, Figure S6). K_D values for Pu adsorption to each clay suspension are presented as a function of equilibration time in Figure 8c. Pu uptake does not significantly evolve over the first month, with an average distribution coefficient for all dispersions of log (K_D (dm^3/kg)) = 5.7 ± 0.5. Although, the Pu(IV) surface complexation constants for the 2 SPNE SC/CE model used in this study were based on several approximations, the predicted log (K_D (dm^3/kg)) = 6.3 (dashed line in Figure 8c) agrees well with the experimental data. High uptake of Pu show that Pu(IV) predominated in the SGW. However, the uptake was slightly lower than for Th (Figure 7c) and the slight increase in uptake of Pu over time (almost insignificant given the error bars) might suggest the presence of a small fraction of Pu(III), as present initially, which took time to oxidize to Pu(IV). After 6 months equilibration time, the uptake of Pu was similar to those reported for Th and those predicted from the model. They indicate a consistent high adsorption of the two tetravalent RNs. Previous studies (Geckeis et al., 2004; Huber et al., 2015) reported log (K_D (dm^3/kg)) = 5.4 ± 0.5 and log (K_D (dm^3/kg)) = 6.4 ± 0.5 in ground waters of low ionic strength (~1 mM) and pH = 9.5 – 9.6 for adsorption of Pu(IV) to montmorillonite. These values were consistent with the present work despite higher Eh in our study (0 to -200 mV in (Geckeis et al., 2004; Huber et al., 2015)), due to the large stability field of Pu(IV) at pH ≈ 9.

As for Th, we observe a lower Pu uptake onto the clay in the $S3.5^{UC,FA}$ dispersion since FA was acting as a competing ligand (Figure 8c). Pu adsorption in the presence of FA remained constant at log (K_D (dm^3/kg)) = 5.1 ± 0.5. In previous published work, the reported competitive effect of added FA differs. Thus, Ticknor et al. (Ticknor et al., 1996) investigated Pu uptake by montmorillonite ([Pu(IV)] = $1.1 \cdot 10^{-10}$ M, m/V = 25 g/L) in the presence of FA (0 – 4.84 mg/L) at pH = 7.7, with 56 mg/L HCO_3 and an ionic strength of ~0.2 M, and observed a maximum decrease in log (K_D (dm^3/kg)) from ~4.8 to ~3.5, even though their FA to montmorillonite ratio was far less than in our study. On the opposite, Boggs et al. (Boggs et al., 2015) did not find any effect of FA addition at pH = 8 in 0.01 M NaCl. In that study, the FA to montmorillonite ratio was higher (m/V = 0.1 g/L, [FA] = 1.5 mg/L, [Pu(IV)] = 10^{-10} M). A decrease in Pu adsorption was expected under our conditions as suggested by the Th

results (Figure 7c) and similar studies with gibbsite, FA and Pu(IV) at pH 8 – 10 in 0.1 M NaCl (Simpkins, 2011).

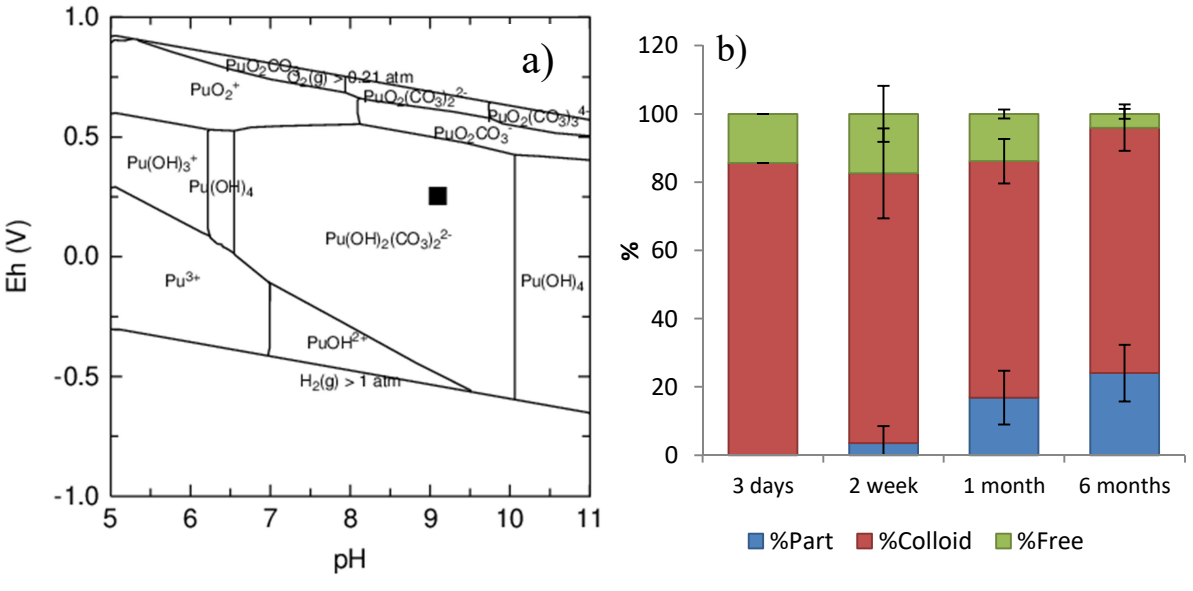

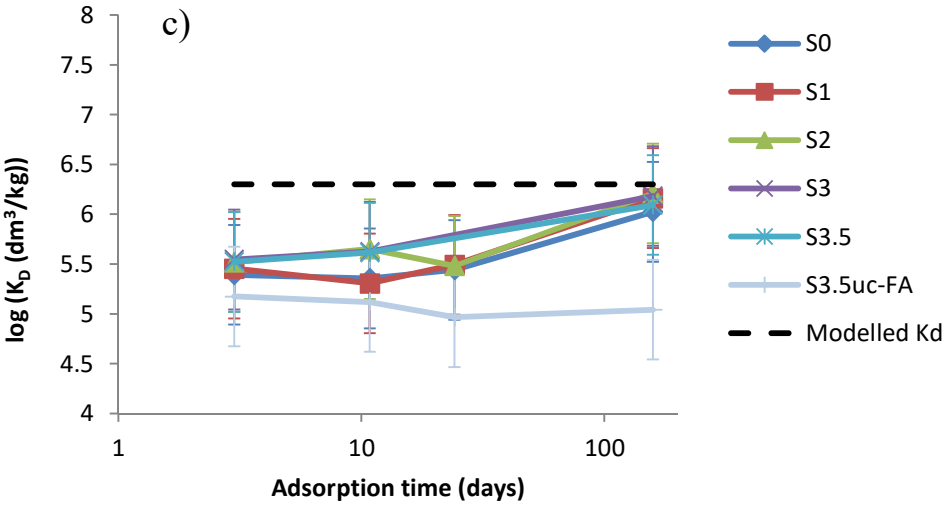

Figure 8: a) Predominance pH-Eh diagram for Pu in the SGW. The experimental conditions are marked by a black square (pH = 8.9 and Eh = 230 mV). b) Histograms presenting the distribution of Pu, in percentage, between particulates (%Part, blue), stable clay colloids (%Colloid, red) or soluble species (%Free, green) in the S0 dispersion, shown for different equilibration times. The results obtained for the other clay dispersions are presented in the Supporting Information (SIF -7, Figure S6). c) Adsorption of Pu for all different sized montmorillonite dispersions, expressed as log (K_D (dm^3/kg)) values as a function of equilibration time. The dashed line corresponds to the predicted Pu adsorption from modelling.

548

549 ### 3.2 Discussion of colloidal size effect on adsorption of RNs onto montmorillonite

550 The present batch adsorption results do not suggest that any of the tested clay colloid
551 dispersions particularly favour adsorption of Th(IV) and Pu(IV), within the analytical
552 uncertainties (see Figures 7c and 8c where the uptake of Th and Pu was normalized to the
553 mass of montmorillonite and expressed as log K_D according to equation 1). To better compare
554 the amount of adsorbed RNs, the estimated amounts of edge sites were calculated by
555 assuming disc-shaped particles with a given mean particle size (Norrfors et al., 2015). The
556 estimates for each clay dispersion are included in Table 1, which suggests an increase by a
557 factor of approximately six in the amount of sites (corresponding to both weak and strong
558 sites according to the 2 SPNE SC/CE model) between the dispersions containing all the clay
559 particle sizes (S0) and those more restricted to smaller sizes ($S3.5^{UC}$). Based on these
560 estimations, a factor six difference in the amount of adsorbed RNs could be expected. K_D
561 values normalized to the amount of sites ($K_{D,sites}$), instead of mass, could be calculated using
562 equation 2. This yielded a maximal theoretical difference of log(6) = 0.8 units between the
563 two dispersions S0 and S3.5. Nevertheless, this value was similar to the experimental
564 uncertainty (± 0.5 units) for log K_D measurements, and could explain why no significant
565 difference in adsorption between the clay dispersions could be detected in our study.

566 To better compare the adsorption onto smaller and larger clay colloids, K_D values for the
567 montmorillonite pertaining to the particulate phase ($K_{D,part}$, for the larger particles) were
568 calculated, using equation 3. This $K_{D,part}$ value can be compared to the K_D value of stable,
569 suspended montmorillonite colloids (corresponding to smaller colloids). All clay dispersions
570 were polydisperse and in the dispersions with the largest sized colloids, the smaller sized
571 colloids were present as well. From the amount of settled colloids (Figure 3), compared to the
572 amount of Th in the particulate phase in dispersion S0 after 6 months (Figure 7b), a log
573 ($K_{D,part}$ (dm^3/kg)) = 6.2 ± 0.5 was obtained. This was similar to log (K_D (dm^3/kg)) = 6.3 ± 0.5
574 obtained for the smaller, stable dispersion S3.5, within the experimental uncertainties.
575 Consequently, the amount of adsorbed Th was similar for both clay dispersions and no
576 difference in K_D values related to the mean colloidal size in the clay dispersions could be
577 inferred.

578 To summarize, no significant differences between adsorption of strongly adsorbing RNs onto
579 the smallest and largest sized montmorillonite colloids could be deduced, so that an "average

log (K_D)" should provide sufficient estimates for RN adsorption to bentonites. This "average log (K_D)" can be used in reactive transport modelling with confidence, which simplifies models for RN migration accordingly. To better study a potential effect of colloidal size, one may recommend the use of RNs which adsorb to clays stronger than penta- hexa- and heptavalent RNs but weaker than tetravalent RNs.

While an ultimate statement concerning desorption properties related to the mean colloidal (particle) size for the added RNs cannot be made, an effect did occur for natural ^{238}U which varied significantly with the clay dispersion properties (see Supporting Information, SIF-4).

4 Conclusions

In this work, experiments were performed on RN uptake onto size separated montmorillonite colloids. Np(V), Tc(VII) and U(VI) were found not to adsorb onto montmorillonite under the present experimental conditions. Instead, they were present as soluble species, mainly as $NpO_2CO_3^-{}_{(aq)}$, $TcO_4^-{}_{(aq)}$ and $UO_2(CO_3)_3^{4-}{}_{(aq)}$, respectively. On the contrary, Th(IV) and Pu(IV) strongly adsorb onto montmorillonite. If fulvic acids are present (as here during the fractionation step of the clay colloids and after the dilution of their dispersions), the amount Pu and Th associated with clay was significantly decreased. During the experimental observation period (up to 6 months), larger clay particles settled with time. A part of Th and Pu were adsorbed and remain adsorbed on these larger, unstable montmorillonite particles (i.e. in the particulate phase). All experimental results were in line with model predictions.

No difference in adsorption behaviour of Th and Pu onto different sized clay colloids, expressed as mass-normalized K_D values, was found. Between the clay dispersions with smallest and the largest mean colloidal sizes, an estimated difference by a factor of six in the amounts of edge sites was calculated. This was too small to be detectable within the experimental uncertainties. Therefore, based on the experimental results for MX-80 presented here, it seems to be valid to implement an "average log K_D" for all colloidal sizes in reactive transport modelling codes.

While a variation in the montmorillonite colloidal size does not seem to influence the adsorption behaviour of strongly adsorbing RNs, the question remains if it affects RN desorption and desorption kinetics. This is presently investigated in a separate study.

610

611 Acknowledgements

612 The Swedish Nuclear Fuel and Waste Management Co. (SKB) is gratefully acknowledged for
613 generous financial support. This work is a part of the project CP-BELBaR Fission 2010-1.1.1.
614 This work has been supported by the European FP7 TALISMAN (**T**ransnational **A**ccess to
615 **L**arge **I**nfrastructure for a **S**afe **M**anagement of **A**cti**N**ide) project under the grant agreement #
616 323300; JRP no TALI-C02-10. The authors gratefully acknowledge C. Walschburger
617 (Institute for Nuclear Waste Disposal) for laboratory work and analytical support.

References

THEREDA, Thermodynamic Reference Database. Release 2013-08-02. .

Alliot, I., Alliot, C., Vitorge, P., Fattahi, M., 2009. Speciation of Technetium(IV) in Bicarbonate Media. Environmental Science & Technology 43, 9174-9182.

Altmaier, M., Gaona, X., Fellhauer, D., Buckau, G., 2010. Intercomparison of redox determination methods on designed and near-neutral aqueous systems; KIT-SR 7572. Karlsruhe Institute of Technology, Karlsruhe 34.

Altmaier, M., Neck, V., Fanghänel, T., 2004. Solubility and colloid formation of Th(IV) in concentrated NaCl and MgCl2 solution, Radiochimica Acta/International journal for chemical aspects of nuclear science and technology, p. 537.

Bernhard, G., Geipel, G., Reich, T., Brendler, V., Amayri, S., Nitsche, H., 2001. Uranyl(VI) carbonate complex formation: Validation of the Ca2UO2(CO3)3(aq.) species. Radiochim. Acta 89, 511-518.

Boggs, M.A., Dai, Z., Kersting, A.B., Zavarin, M., 2015. Plutonium(IV) sorption to montmorillonite in the presence of organic matter. Journal of Environmental Radioactivity 141, 90-96.

Bouby, M., Geckeis, H., Lutzenkirchen, J., Mihai, S., Schafer, T., 2011. Interaction of bentonite colloids with Cs, Eu, Th and U in presence of humic acid: A flow field-flow fractionation study. Geochim. Cosmochim. Acta 75, 3866-3880.

Bradbury, M.H., Baeyens, B., 2005. Modelling the sorption of Mn(II), Co(II), Ni(II), Zn(II), Cd(II), Eu(III), Am(III), Sn(IV), Th(IV), Np(V) and U(VI) on montmorillonite: Linear free energy relationships and estimates of surface binding constants for some selected heavy metals and actinides. Geochim. Cosmochim. Acta 69, 875-892.

Bradbury, M.H., Baeyens, B., 2006. Modelling sorption data for the actinides Am(III), Np(V) and Pa(V) on montmorillonite. Radiochim. Acta 94, 619-625.

Bradbury, M.H., Baeyens, B., 2009. Sorption modelling on illite. Part II: Actinide sorption and linear free energy relationships. Geochim. Cosmochim. Acta 73, 1004-1013.

Bradbury, M.H., Baeyens, B., 2011. Predictive sorption modelling of Ni(II), Co(II), Eu(IIII), Th(IV) and U(VI) on MX-80 bentonite and Opalinus Clay: A “bottom-up” approach. Applied Clay Science 52, 27-33.

Bradford, S.A., Yates, S.R., Bettahar, M., Simunek, J., 2002. Physical factors affecting the transport and fate of colloids in saturated porous media. Water Resources Research 38, 63-61-63-12.

Geckeis, H., Schäfer, T., Hauser, W., Rabung, T., Missana, T., Degueldre, C., Möri, A., Eikenberg, J., Fierz, T., Alexander, W.R., 2004. Results of the colloid and radionuclide retention experiment (CRR) at the Grimsel Test Site (GTS), Switzerland – impact of reaction kinetics and speciation on radionuclide migration. Radiochim. Acta 92, 765-774.

Guillaumont, R., Mompean, F.J., 2003. Update on the chemical thermodynamics of uranium, neptunium, plutonium, americium and technetium, in: Mompean, F.J., Illemassene, M., Domenech-Orti, C., Said, K.B. (Eds.). OECD Nuclear Energy Agency, Data Bank, Issy-les-Moulineaux, France.

Hartmann, E., Geckeis, H., Rabung, T., Lützenkirchen, J., Fanghänel, T., 2008. Sorption of radionuclides onto natural clay rocks, Radiochimica Acta International journal for chemical aspects of nuclear science and technology, p. 699.

Holmboe, M., Jonsson, M., Wold, S., 2012. Influence of γ-radiation on the reactivity of montmorillonite towards H2O2. Radiation Physics and Chemistry 81, 190-194.

Huber, F., Kunze, P., Geckeis, H., Schäfer, T., 2011. Sorption reversibility kinetics in the ternary system radionuclide–bentonite colloids/nanoparticles–granite fracture filling material. Applied Geochemistry 26, 2226-2237.

Huber, F.M., Heck, S., Truche, L., Bouby, M., Brendle, J., Hoess, P., Schafer, T., 2015. Radionuclide desorption kinetics on synthetic Zn/Ni-labeled montmorillonite nanoparticles. Geochim. Cosmochim. Acta 148, 426-441.

Jennings, B.R., 1993. Size and thickness measurement of polydisperse clay samples. Clay Minerals 28, 485-494.

672 Jennings, B.R., Parslow, K., 1988. Particle Size Measurement: The Equivalent Spherical
673 Diameter. Proceedings of the Royal Society of London. A. Mathematical and Physical
674 Sciences 419, 137-149.

675 Karnland, O., Olsson, S., Nilsson, U., 2006. Mineralogy and sealing properties of various
676 bentonites and smectite-rich clay materials. SKB internal report TR-06-30.

677 Kinniburgh, D.G., Cooper, D.M., 2009. PhreePlot: Creating graphical output with
678 PHRREQC.

679 Kirsch, R., Fellhauer, D., Altmaier, M., Neck, V., Rossberg, A., Fanghänel, T., Charlet, L.,
680 Scheinost, A.C., 2011. Oxidation State and Local Structure of Plutonium Reacted with
681 Magnetite, Mackinawite, and Chukanovite. Environmental Science & Technology 45, 7267-
682 7274.

683 Kunze, P., Seher, H., Hauser, W., Panak, P.J., Geckeis, H., Fanghänel, T., Schäfer, T., 2008.
684 The influence of colloid formation in a granite groundwater bentonite porewater mixing zone
685 on radionuclide speciation. Journal of Contaminant Hydrology 102, 263-272.

686 Latrille, C., Ly, J., Herbette, M., 2006. Retention of Sn(IV) and Pu(IV) onto four argillites
687 from the Callovo–Oxfordian level at Bure (France) from eight equilibrated sedimentary
688 waters, Radiochim. Acta, p. 421.

689 Lujanienė, G., Motiejūnas, S., Šapolaitė, J., 2007. Sorption of Cs, Pu and Am on clay
690 minerals. J. Radioanal. Nucl. Chem. 274, 345-353.

691 Madden, A.S., Hochella, M.F., Luxton, T.P., 2006. Insights for size-dependent reactivity of
692 hematite nanomineral surfaces through Cu2+ sorption. Geochim. Cosmochim. Acta 70, 4095-
693 4104.

694 Marques Fernandes, M., Baeyens, B., Dähn, R., Scheinost, A.C., Bradbury, M.H., 2012.
695 U(VI) sorption on montmorillonite in the absence and presence of carbonate: A macroscopic
696 and microscopic study. Geochim. Cosmochim. Acta 93, 262-277.

697 Marsac, R., Banik, N.l., Lützenkirchen, J., Marquardt, C.M., Dardenne, K., Schild, D., Rothe,
698 J., Diascorn, A., Kupcik, T., Schäfer, T., Geckeis, H., 2015. Neptunium redox speciation at
699 the illite surface. Geochim. Cosmochim. Acta 152, 39-51.

Missana, T., Alonso, Ú., Turrero, M.J., 2003. Generation and stability of bentonite colloids at the bentonite/granite interface of a deep geological radioactive waste repository. Journal of Contaminant Hydrology 61, 17-31.

Missana, T., Geckeis, H., 2006. Grimsel Test Site – Investigation Phase V. The CRR Final Project Report Series II: Supporting Laboratory Experiments with Radionuclides and Bentonite Colloids NAGRA Technical Report Series NTB 03-02.

Möri, A., Alexander, W.R., Geckeis, H., Hauser, W., Schafer, T., Eikenberg, J., Fierz, T., Degueldre, C., Missana, T., 2003. The colloid and radionuclide retardation experiment at the Grimsel Test Site: influence of bentonite colloids on radionuclide migration in a fractured rock. Colloids and Surfaces a-Physicochemical and Engineering Aspects 217, 33-47.

Neck, V., Kim, J.I., Kanellakopulos, B., 1992. Solubility and Hydrolysis Behaviour of Neptunium(V). Radiochimca Acta 56, 25–30.

Norrfors, K.K., Bouby, M., Heck, S., Finck, N., Marsac, R., Schäfer, T., Geckeis, H., Wold, S., 2015. Montmorillonite colloids: I. Characterization and stability of dispersions with different size fractions. Applied Clay Science 114, 179-189.

Pan, D.-Q., Fan, Q.-H., Li, P., Liu, S.-P., Wu, W.-S., 2011. Sorption of Th(IV) on Na-bentonite: Effects of pH, ionic strength, humic substances and temperature. Chemical Engineering Journal 172, 898-905.

Parkhurst, D.L., Appelo, C.A.J., 1999. User's guide to PHREEQC (version 2). US Geol. Surv. Water Resour. Inv. Rep. 99-4259, 312p. .

Rand, R., Fuger, J., Neck, V., Grenthe, I., Rai, D., 2009. Chemical Thermodynamics of Thorium, Chemical Thermodynamics, vol. 11. OECD Publishing

Rard, J.A., 1999. Chemical thermodynamics of technetium. North Holland.

Regenspurg, S., Schild, D., Schäfer, T., Huber, F., Malmström, M.E., 2009. Removal of uranium(VI) from the aqueous phase by iron(II) minerals in presence of bicarbonate. Applied Geochemistry 24, 1617-1625.

Runde, W., Conradson, S.D., Wes Efurd, D., Lu, N., VanPelt, C.E., Tait, C.D., 2002. Solubility and sorption of redox-sensitive radionuclides (Np, Pu) in J-13 water from the

728 Yucca Mountain site: comparison between experiment and theory. Applied Geochemistry 17,
729 837-853.

730 Schäfer, T., Huber, F., Seher, H., Missana, T., Alonso, U., Kumke, M., Eidner, S., Claret, F.,
731 Enzmann, F., 2012. Nanoparticles and their influence on radionuclide mobility in deep
732 geological formations. Applied Geochemistry 27, 390-403.

733 Simpkins, L., 2011. Influence of natural organic matter on plutonium sorption to gibbsite.

734 Sirivithayapakorn, S., Keller, A., 2003. Transport of colloids in saturated porous media: A
735 pore-scale observation of the size exclusion effect and colloid acceleration. Water Resources
736 Research 39, n/a-n/a.

737 SKB, 2010. Design and production of the KBS-3 repository. SKB internal report TR-10-12.

738 Stul, M.S., Van Leemput, L., 1982. Particle-size distribution, cation exchange capacity and
739 charge density of deferrated montmorillonites. Clay Minerals 17, 209-215.

740 Ticknor, K.V., Vilks, P., Vandergraaf, T.T., 1996. The effect of fulvic acid on the sorption of
741 actinides and fission products on granite and selected minerals. Applied Geochemistry 11,
742 555-565.

743 Tournassat, C., Neaman, A., Villiéras, F., Bosbach, D., Charlet, L., 2003. Nanomorphology of
744 montmorillonite particles: Estimation of the clay edge sorption site density by low-pressure
745 gas adsorption and AFM observations. Am. Miner. 88, 1989-1995.

746 Turner, D.R., Pabalan, R.T., Bertetti, F.P., 1998. Neptunium(V) sorption on montmorillonite;
747 an experimental and surface complexation modeling study. Clay Clay Min. 46, 256-269.

748 Vahlund, F., Hermansson, H., 2006. A direct numerical approach to solving the transport
749 equations for radionuclide transport in fractured rock. SKB internal report R-04-50.

750 White, G.N., Zelazny, L.W., 1988. Analysis and implications of the edge structure of
751 dioctahedral phyllosilicates. Clay Clay Min. 36, 141-146.

752 Wolf, M., Buckau, G., Geyer, S., 2004. Isolation and characterisation of new batches of
753 GoHy-573 humic and fulvic acids., in: ed., G.B. (Ed.), Humic substances in performance
754 assessment of nuclear waste disposal: Actinide and iodine migration in the far-field.
755 Wissenschaftliche Berichte FZKA 6969, Forschungszentrum Karlsruhe, pp. 111–124.

Wu, T., Amayri, S., Drebert, J., Loon, L.R.V., Reich, T., 2009. Neptunium(V) Sorption and Diffusion in Opalinus Clay. Environmental Science & Technology 43, 6567-6571.

Yu, S.M., Chen, C.L., Chang, P.P., Wang, T.T., Lu, S.S., Wang, X.K., 2008. Adsorption of Th(IV) onto Al-pillared rectorite: Effect of pH, ionic strength, temperature, soil humic acid and fulvic acid. Applied Clay Science 38, 219-226.

Zhang, W., Tang, X., Weisbrod, N., Guan, Z., 2012. A review of colloid transport in fractured rocks. J. Mt. Sci. 9, 770-787.

Zhao, P., Zavarin, M., Kersting, A., Carroll, S., 2011. Sorption and Precipitation of Plutonium in the Presence of Goethite at Elevated Temperatures. Lawrence Livermore National Laboratory (LLNL), Livermore, CA.

Östhols, E., Bruno, J., Grenthe, I., 1994. On the influence of carbonate on mineral dissolution: III. The solubility of microcrystalline ThO2 in CO2-H2O media. Geochim. Cosmochim. Acta 58, 613-623.